Received: 29 January 2024 | Revised: 17 May 2024 | Accepted: 15 June 2024

DOI: 10.1002/bit.28788

ARTICLE

BIOTECHNOLOGY AND BIOENGINEERING WILEY

3D imaging and analysis to unveil the impact of microparticles on the pellet morphology of filamentous fungi

Anna Dinius[1,2] | Henri Müller[3] | Diana Kellhammer[3] | Charlotte Deffur[3] | Stefan Schmideder[3] | Jörg U. Hammel[4] | Rainer Krull[1,2] | Heiko Briesen[3]

[1]Institute of Biochemical Engineering, Technische Universität Braunschweig, Braunschweig, Germany

[2]Center of Pharmaceutical Engineering, Technische Universität Braunschweig, Braunschweig, Germany

[3]School of Life Sciences, Process Systems Engineering, Technical University of Munich, Freising, Germany

[4]Helmholtz-Zentrum hereon, Institute of Materials Physics, Geesthacht, Germany

Correspondence
Heiko Briesen, Chair of Process Systems Engineering, Technical University of Munich, Gregor-Mendel-Str. 4, 85354 Freising, Germany.
Email: heiko.briesen@tum.de

Funding information
Deutsches Elektronen-Synchrotron; SPP 1934 DiSPBiotech—31547657; SPP 1934 DiSPBiotech—315305620; Helmholtz-Zentrum Hereon; SPP 2170 InterZell—427889137; SPP 1934 DiSPBiotech—315384307; Deutsche Forschungsgemeinschaft

Abstract

Controlling the morphology of filamentous fungi is crucial to improve the performance of fungal bioprocesses. Microparticle-enhanced cultivation (MPEC) increases productivity, most likely by changing the fungal morphology. However, due to a lack of appropriate methods, the exact impact of the added microparticles on the structural development of fungal pellets is mostly unexplored. In this study synchrotron radiation-based microcomputed tomography and three-dimensional (3D) image analysis were applied to unveil the detailed 3D incorporation of glass microparticles in nondestructed pellets of *Aspergillus niger* from MPEC. The developed method enabled the 3D analysis based on 375 pellets from various MPEC experiments. The total and locally resolved volume fractions of glass microparticles and hyphae were quantified for the first time. At increasing microparticle concentrations in the culture medium, pellets with lower hyphal fraction were obtained. However, the total volume of incorporated glass microparticles within the pellets did not necessarily increase. Furthermore, larger microparticles were less effective than smaller ones in reducing pellet density. However, the total volume of incorporated glass was larger for large microparticles. In addition, analysis of MPEC pellets from different times of cultivation indicated that spore agglomeration is decisive for the development of MPEC pellets. The developed 3D morphometric analysis method and the presented results will promote the general understanding and further development of MPEC for industrial application.

KEYWORDS

Aspergillus niger, computed tomography, filamentous fungi, microparticle-enhanced cultivation, pellet growth, synchrotron radiation

1 | INTRODUCTION

Filamentous fungi have been used in industrial biotechnology for over a 100 years (Cairns et al., 2018). In nature, they efficiently degrade biomass and ensure their survival by biosynthesizing valuable primary and secondary metabolites (Wösten, 2019). These capabilities have been harnessed by industrial biotechnology to produce enzymes, such as cellulases, organic acids like citric acid (primary metabolite), or antibiotics, such as penicillin (secondary metabolite) (Cairns et al., 2019; Füting et al., 2021). Depending on the

Anna Dinius and Henri Müller contributed equally to this study.

submerged cultivation conditions, the observed biomass morphology varies from freely dispersed mycelia to nearly spherical pellets consisting of branched and partially intertwined hyphae forming a network of varying density. The morphology strongly affects bioprocess performance (product titer, productivity, and product yield) (Veiter et al., 2018). In general, the product yield depends on the oxygen and nutrient supply, which in turn depends on the morphology of the filamentous microorganisms (Cairns et al., 2019; Schmideder et al., 2021). It has been shown that the morphology of small, low-density pellets, which favors low viscosity and Newtonian behavior of the culture broth and adequate oxygen and nutrient supply of the microorganism, is often preferred over dispersed mycelia (Antecka, Bizukojc, & Ledakowicz, 2016; Krull et al., 2013; Posch et al., 2012). However, enzyme production, for example, pectinase, in *Aspergillus niger* can be an example for dispersed mycelium being favorable (Colin et al., 2013; Kaup et al., 2008). Although rapid biomass accumulation can be achieved with dispersed mycelia, this morphology results in a highly viscous culture broth that limits nutrient delivery and requires high energy input for mixing (Antecka, Bizukojc, & Ledakowicz, 2016; Wucherpfennig et al., 2010). Thus, analyzing and controlling the morphology of filamentous fungi is crucial to improve the performance of fungal bioprocesses.

In recent years, image analysis methods based on three-dimensional (3D) imaging with microcomputed tomography (μ-CT) have been developed for detailed exploration of the entire nondestructed fungal pellet micromorphology (Schmideder, Barthel, Friedrich, et al., 2019) and analysis of the diffusive mass transfer of nutrients within fungal pellets (Schmideder, Barthel, Müller, et al., 2019; Schmideder et al., 2021). The use of synchrotron radiation-based μ-CT (SR-μ-CT) instead of laboratory-scale μ-CT increased the sample throughput, resulting in statistically meaningful micromorphological data of many fungal pellets over the cultivation period (Müller et al., 2023).

Different morphology engineering approaches have been devised to create defined pellet morphologies for enhanced process performance (Böl et al., 2021; Krull et al., 2013). For instance, changing the concentration of spore inoculum (Bizukojc & Ledakowicz, 2010; Papagianni & Mattey, 2006), pH (Colin et al., 2013), osmolality (Wucherpfennig et al., 2011), and agitation and aeration (Lin et al., 2010) in the cultivation medium force the development of small pellets during submerged cultivation. One promising morphology engineering approach includes the addition of microparticles, which has already been used at the laboratory scale (Driouch, Sommer, & Wittmann, 2010; Kaup et al., 2008).

In the past, various types of particles were utilized for microparticle-enhanced cultivations (MPEC) in filamentous fungal or bacterial cultivations. Generally, MPEC has been associated with increased product yields, as discussed in several recent review articles (Antecka, Bizukojc, & Ledakowicz, 2016; Böl et al., 2021; Dinius, Kozanecka, et al., 2023; Laible et al., 2021). In this context, the effects of microparticles are multifaceted. For spore-agglomerating species, it has been hypothesized that interactions between microparticles and spores disturb the initial spore agglomeration process, which is crucial for the subsequent pellet formation. Consequently, smaller pellets can be found in the culture broth (Antecka, Blatkiewicz, Bizukojć, & Ledakowicz, 2016; Driouch, Sommer, & Wittmann, 2010; Yatmaz et al., 2016). Another benefit is hypothesized to be the incorporation of microparticles into the hyphal network of these pellets. Here, they act as spacer-like obstacles, enhancing the pellets' porosity and effective diffusivity (Dinius, Schrinner et al., 2023; Gonciarz & Bizukojc, 2014). Both mechanisms lead to higher mycelium activity or a higher proportion of active biomass in the pellets, sufficiently supplied with the growth-limiting substrate oxygen or further nutrients (Driouch, Roth, et al., 2010; Driouch et al., 2012; Gonciarz & Bizukojc, 2014). By selecting a suitable microparticle setup, tailored adjustments to pellet morphology can be made. Thereby, achieving improved product synthesis is currently feasible up to lab-scale bioreactors (Driouch et al., 2012; Gürler et al., 2021; Yatmaz et al., 2020). To the best of our knowledge, a further scale-up to an industrial-scale bioreactor has not yet been reported.

However, previous studies have described the impact of MPEC on fungal strains, primarily employing talc or aluminum oxide as microparticles. As summarized and discussed in Laible et al. (2021), these types of particles can exhibit significant variations in morphological characteristics and physicochemical properties. Consequently, the biochemical and physical interactions of these microparticles with their environment, such as with hyphae or the cultivation medium, can lead to high variability among bioprocesses (Laible et al., 2021). For this reason, glass microparticles have recently been introduced as a novel and effective microparticle system for MPEC in filamentous bacteria (Dinius, Schrinner, et al., 2023). The advantages of choosing glass microparticles include their relative thermal and chemical stability, as well as their homogeneous spherical shape, which eliminates the needs for considering shapes dependent intercalation characteristics. Thus, in the present study, glass microparticles were used for the first time for MPEC experiments involving the cultivation of filamentous fungi. Specifically, the recombinant strain *Aspergillus niger* SKAn1015, known for producing the enzyme fructofuranosidase was employed. This strain had been previously discussed in the context of MPEC and other morphology engineering approaches (Driouch, Roth, et al., 2010; Driouch, Sommer, & Wittmann 2010; Driouch et al., 2012; Wucherpfennig et al., 2011).

Furthermore, SR-μ-CT and subsequent 3D image analysis were used to analyze pellets from MPEC cultivations. The developed image analysis can detect the incorporated glass microparticles within *A. niger* pellets. This method makes it possible to localize the microparticles and quantify the volume of glass microparticles in whole, nondestructed fungal pellets for the first time. Until now, this was not achievable with the conventional methods based on microtome pellet slicing and confocal laser scanning microscopy (CLSM), which only offer two dimensional (2D) or 3D insights of thin pellet slices at a low-throughput level. However, using SR-μ-CT for 3D imaging enabled the convenient analysis based on 375 nondestructed pellets from different MPEC cultivations.

With the developed method, we analyzed the effect of glass microparticles on product synthesis and the impact of glass microparticles on the 3D pellet macro- and micromorphology. The examinations include: (1) the effects of microparticle concentration, (2) the time-resolved effect of microparticles during a cultivation process, and (3) the influence of microparticle size on fungal pellets. These examinations serve to introduce our developed method and reproduce the results of existing MPEC studies with a statistically significant number of examined pellets. In addition, the data generated with the new method can now quantify parameters such as the stored glass volume for many nondestructed individual pellets, which was not possible in previous studies.

2 | MATERIALS AND METHODS

2.1 | Used microparticles

For the MPEC experiments, talc powder (10 µm, Sigma-Aldrich GmbH), aluminum oxide (anhydrous, Merck KGaA), and soda-lime glass microparticles (SOLID Micro Glass Beads, type S, $x = 0–20$ and 0–50 µm; Sigmund Lindner GmbH) were used. Particle size analysis was conducted using laser diffraction (Mastersizer 3000 Malvern Panalytical Ltd.). Mean particle sizes were determined; $x_{50,3} = 7.9$ µm ($x_{10,3} = 0.9$ µm, $x_{90,3} = 16.3$ µm) and $x_{50,3} = 30.5$ µm ($x_{10,3} = 15.0$ µm, $x_{90,3} = 50.5$ µm) for glass microparticles; $x_{50,3} = 7.0$ µm ($x_{10,3} = 1.48$ µm, $x_{90,3} = 18$ µm) for talc microparticles; $x_{50,3} = 13.7$ µm ($x_{10,3} = 5.11$ µm, $x_{90,3} = 30.7$ µm) (Driouch, Sommer, & Wittmann, 2010) for aluminum oxide microparticles. In the following, the glass microparticles will be referred to as "small" microparticles ($x_{50,3} = 7.9$ µm) and "large" microparticles ($x_{50,3} = 30.5$ µm), corresponding to their median particle diameters.

2.2 | Cultivation, sampling, and preparation of pellets

In this study, the recombinant strain *A. niger* SKAn1015 was used. It was derived from *A. niger* AB1.13 through transformation and carries the *suc1* (fructofuranosidase, EC 3.2.1.26) gene for fructofuranosidase production under the constitutive *pkiA* (pyruvate kinase) promotor (Driouch, Sommer, & Wittmann, 2010; Zuccaro et al., 2008). For the spore inoculum preparation, spores were grown (72 h, 30°C) on agar plates (30 g/L potato dextrose agar, 10 g/L agar) and harvested by adding 10-mL NaCl solution (0.9%) and gently scrubbing with a cotton stick. The resulting spore solution was filtrated (miracloth, pore size 25 µm, Calbiochem, Frankfurt am Main, Germany).

250-mL Erlenmeyer flasks equipped with four baffles were used for submerged cultivations. For MPEC experiments, the respective amount of microparticles and 3 mL of MilliQ® water were added to the flasks before autoclaving. In control cultures (without microparticles) only MilliQ® water was added. After autoclaving, the basic medium, as described in (Driouch, Sommer, & Wittmann, 2010) (with 20-g/L sucrose instead of glucose), was added to achieve a total volume of 50 mL. The culture was then inoculated at a concentration of 1×10^6 spores/mL, and incubation was performed on a rotary shaker (Certomat BS-1, Sartorius) in the dark, in duplicates, at 37°C, 120 1/min with a 50-mm amplitude. For one time-resolved experiment, samples were taken every 24 h, while all other experiments were terminated and sampled after 72 h. For SR-µ-CT measurements, 2 mL of *A. niger* containing culture broth were isolated and transferred to a 2-mL reaction tube. A previously developed protocol (Müller et al., 2023; Schmideder, Barthel, Friedrich, et al., 2019) was used to wash and freeze-dry the pellets.

2.3 | Analytical measurements

For analytical quantification, 2 mL of the culture broth were centrifuged (13,000 1/min, 1 min), filtered (Minisart 0.2 µm, Sartorius) and stored (−20°C) until analysis. The fructofuranosidase activity was determined following a method similar to the one described by (Driouch, Sommer, & Wittmann, 2010) using a thermo cycler (Mastercycler, Eppendorf). Briefly, 20 µL of the filtered samples were mixed with 100 µL of 1.65-M sucrose (in 0.05-M phosphate buffer, pH 5.4) in a lockable reaction tube to initiate the enzymatic reaction. After incubation (30 min, 40°C), the reaction was stopped by heating the mixture to 99°C for 10 min. Following cooling, the mixture was centrifuged (13,000 1/min, 10 min, 4°C). The glucose concentration resulting from the enzymatic cleavage of sucrose was quantified by HPLC, as described in (Schrinner et al., 2020). Negative controls were performed using samples with heat-inactivated fructofuranosidase. For substrate quantification in the culture broth, analysis was conducted by HPLC similar to glucose quantification for enzyme activity measurement. Measurements were performed in duplicates (two flasks for each condition).

2.4 | Synchrotron microcomputed tomography

SR-µ-CT was conducted at the Imaging Beamline P05 (Greving et al., 2014; Haibel et al., 2010; Wilde et al., 2016) operated by the Helmholtz-Zentrum hereon at the PETRA III storage ring (Deutsches Elektronen-Synchrotron—DESY). For the 3D imaging, the freeze-dried *A. niger* pellet samples were carefully transferred into standardized sample holders for each cultivation and sampling time (Müller et al., 2023). The sample holders filled with pellets were placed on sample pins and put in the magazine of the sample changing robot, which allowed fast and automatic sample change. Imaging was performed at a photon energy of 17.5 keV with a 100-ms exposure time for each projection. The sample camera distance was set to 50 mm. During each tomographic scan, a 50-MP CMOS camera system with an effective pixel size of 0.47 µm and a field of view of 3.71 mm × 2.33 mm recorded 2401 projections equally spaced between 0 and 180°. For each sample, two scans were performed to increase the field of view in the vertical direction. Including the time for the sample change, one entire sample (one

sample holder, two scans) could be measured within 13 min. Image reconstruction with threefold pixel binning was established with the filtered back projection algorithm implemented in a custom reconstruction pipeline (Moosmann et al., 2014) based on MATLAB (MathWorks) and the Astra Toolbox (Palenstijn et al., 2011; Van Aarle et al., 2015; Van Aarle et al., 2016). After 3D image reconstruction of the lower and upper sample volumes, the images were stitched together by a custom MATLAB stitching algorithm. The resulting sample volume is 2640 × 2640 × 3217 voxels with a binned voxel size of 1.41 µm. The intensity values of the 3D images were represented by floating point numbers, resulting in a size of 83.5 GB for each image. SR-µ-CT measurements of 20 samples were performed from different cultivation and sampling times, resulting in 1.67 TB of 3D image data for analysis.

2.5 | Image processing

The entire image processing was developed in MATLAB (Version R2023a). A captured 3D gray level image represents air, image noise, parts of the sample holder, and pellets with or without glass microparticles. Two main image segmentation steps were performed during the processing: (1) the segmentation of the pellets into individual ones out of the imaged sample holder with multiple pellets and (2) the segmentation of glass microparticles from the individual pellets.

Step (1) is based on the image processing described by (Müller et al., 2023). In short, after removing parts of the sample holder, a marker-controlled watershed segmentation algorithm (Meyer, 1994) was used to segment the pellets from each other. In contrast to the pellet segmentation by (Müller et al., 2023), the entire image was processed and not divided into two subvolumes, as a larger working memory (384 GB) was available.

Since image segmentation errors can occur during the processing, such as over-segmentation resulting in cropped pellets or under-segmentation resulting in improperly separated pellets, the obtained individual gray level pellet images were manually sorted. Here, cropped and not properly separated gray level pellet images were discarded, accounting for 28% (145 discarded pellet images out of 520 segmented pellet objects). The following describes the newly developed segmentation of glass microparticles within pellets.

2.5.1 | Segmentation of glass microparticles

To detect and segment the glass microparticles incorporated within the pellets, the gray value distribution that represents the glass microparticles was first determined. Secondly, based on the determined gray value distribution, a global threshold was computed to binarize the glass into the foreground. A postprocessing step of the segmented glass microparticles terminates the glass microparticle detection. Figure 1a,b shows the final image segmentation results of glass microparticles and hyphal material from gray level pellet images of SR-µ-CT. The developed image analysis pipeline can also be used to segment and analyze the incorporation of aluminum oxide and talc microparticles (Figure 1c,d) within dispersed mycelium and pellets. A detailed description of the segmentation is described below.

The gray value distribution of the glass microparticles was determined by detecting gray values that belong to the internal boundary of the glass microparticles. For this, the pellet gray level image was eroded using a sphere with three voxels in diameter. Using the eroded gray level image, the gradient weights for each image voxel (Matlab function "gradientweight") with a sigma value of 0.5 were computed. The gray intensity values representing glass microparticles were brighter than those representing the background or hyphae of the pellet. Thus, the voxels of the internal glass boundary provided the highest gradients, which in turn represented the lowest gradient weights.

In contrast, smooth gray level regions, such as the background, provided the lowest gradients/highest gradient weights. The gradient weights were scaled to the interval [0, 1]. Subsequently, the resulting image was binarized with a low global threshold of 0.1, as the gradient weights of the inner glass microparticle boundaries were by far the lowest gradient weights (about 0.001), with the next highest gradient weights starting at 0.25. The complement of the binarized image represented the internal glass microparticle boundaries as the foreground voxels. By masking all voxels of the gray level pellet image with zero except for those defining the internal microparticle boundaries, the gray values of the glass microparticles were obtained.

The global threshold T was calculated by $T = \bar{x} - S$, whereby $\bar{x}$ is the arithmetic mean and S the standard deviation of the gray level distribution of glass microparticles. A similar calculation of the global threshold was used by Müller et al. (2023). The pellet gray level image was binarized with the computed threshold, resulting in an image matrix with the glass microparticles as foreground objects.

As a final step, a postprocessing was performed, which included the slice-wise filling of the binarized glass microparticles to fill hollow microparticle regions resulting from air inclusions in the glass. In addition, objects smaller than 27 (3 × 3 × 3) voxels were deleted since it was not certain that these were glass microparticles due to the limited local resolution.

2.5.2 | Determination of local hyphal and glass fractions

The locally resolved hyphal and glass fractions were calculated with the methods described in Schmideder, Barthel, Friedrich, et al., 2019. In short, the segmented gray level pellet images were binarized by setting a global threshold. This global threshold was automatically calculated based on the original gray level image from SR-µ-CT measurements by determining the maximum gray value of the image background (air and image noise) in image regions that did not show parts of the sample holder, pellets, and glass. Such image regions were present at the corners of the µ-CT image. Please note that contrary to (Schmideder, Barthel, Friedrich, et al., 2019) and (Müller et al., 2023) a global threshold that was computed with Otsu's method (Otsu, 1979) could not be used since this threshold was calculated too large for pellets

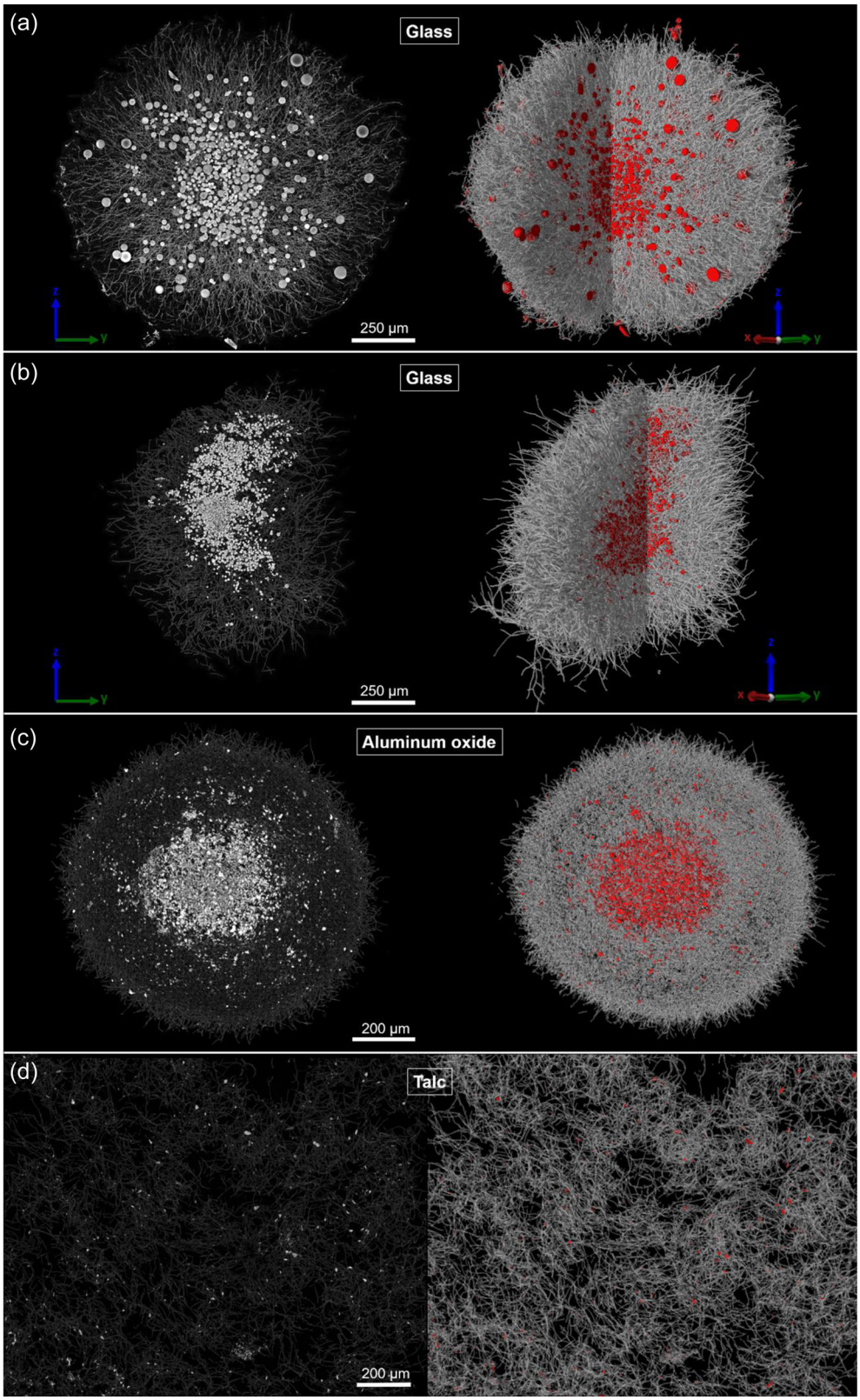

FIGURE 1 Gray level pellet and dispersed mycelium images with different microparticles from synchrotron radiation-based microcomputed tomography measurements (left) and 3D image segmentation results (right) of hyphae (gray color) and microparticles (red color). (a) Pellet from microparticle-enhanced cultivation (MPEC) with large glass microparticles ($x_{50,3}$ = 30.5 µm) at a concentration of 20 g/L. (b) Pellet from MPEC with small glass microparticles ($x_{50,3}$ = 7.9 µm) at a concentration of 20 g/L. The gray level images (left) in (a) and (b) depict maximum intensity projections of pellet slices with a thickness of 30 µm. (c) Pellet from MPEC with aluminum oxide microparticles at a concentration of 10 g/L. (d) Dispersed mycelium from MPEC with talc microparticles at a concentration of 10 g/L. The gray level images (left) in (c) and (d) depict max intensity projections of slices with a thickness of 50 µm. The segmentation results in (c) and (d) show the corresponding slice with a thickness of 50 µm.

supplemented with glass microparticles. The binarized pellet image depicted the pellet's hyphae and glass microparticles as foreground objects. The segmented and binarized glass particles (Section 2.5.-1) were masked in the binarized pellet image to obtain only the hyphae of the pellet. These two binarized images: (1) depicting only the binarized glass microparticles and (2) depicting only the hyphae of the pellet, were used to compute the glass and the hyphal fractions. The local hyphal fractions of a pellet were determined within spherical shells along the distance from the pellet's mass center (Schmideder, Barthel, Friedrich, et al., 2019). The same method was applied to calculate the glass fractions over the pellet's radius using the binarized glass microparticle image. The width of the shells was 15 µm. The hyphal/glass fractions as a function of the pellet's radius were obtained by dividing the volume of hyphae/glass of a shell by the total volume of the corresponding shell. The hyphal/glass fraction near the mass center was calculated within a sphere with a radius of 50 µm.

2.5.3 | Determination of global morphology features

Based on the entire pellet structure, morphological properties were calculated, including the equivalent diameter, the overall solid and hyphal fraction, the total glass volume, the glass fraction, and the aspect ratio of the pellets.

The volume equivalent spherical diameter (VESD) of a pellet was calculated based on the volume of the convex hull $V_{ConvHull}$ of the pellet as $d = \sqrt[3]{\frac{6 \cdot V_{ConvHull}}{\pi}}$. The convex hull $V_{ConvHull}$ is built over the outermost hyphal material of the pellet. The volume of the convex hull is therefore the sum of the total volume of hyphae V_{Hyphae}, the total volume of glass microparticles V_{Glass}, and the total void volume of a pellet. The total volume of hyphae V_{Hyphae} was determined by counting all foreground voxels of the binarized hyphae image (1) without microparticles and multiplying it with the volume per voxel. The same was done to calculate the total volume of the glass microparticles V_{Glass} based on the binarized microparticle image (2). Furthermore, each pellet's overall hyphal, glass, and solid fractions were determined by $\frac{V_{Hyphae}}{V_{ConvHull}}$, $\frac{V_{Glass}}{V_{ConvHull}}$, and $\frac{V_{Hyphae} + V_{Glass}}{V_{ConvHull}}$, respectively. The ratio between the longest and shortest axis of the binarized pellet image defines the aspect ratio of a pellet.

3 | RESULTS AND DISCUSSION

In an initial MPEC experiment, small glass microparticles, along with conventionally used talc and aluminum oxide microparticles (each at 10 g/L), were tested to determine their effectiveness in enhancing the volumetric fructofuranosidase activity in the present cultivation setup. Compared to a nonsupplemented control culture, small glass microparticles exhibited a slightly more favorable effect (+67.4%), surpassing the effect of talc (+47.8%) and aluminum oxide (+19.6%) (Figure 2a). Consequently, glass microparticles are highly suitable for MPEC in filamentous *A. niger* cultivations and confirm their superior effect on product synthesis, which was previously described for secondary metabolite syntheses in filamentous bacteria (Dinius, Schrinner, et al., 2023). Additionally, compared to talc or aluminum oxide, glass microparticles potentially have a minor impact on the cultivation medium and fungal genetics due to secondary effects. For example, glass microparticles are not soluble in the culture medium, so that morphological changes, e.g., are not superimposed by leaching effects, as recently discussed in Laible at al. (2021).

Furthermore, during SR-µ-CT measurements, the glass microparticles enabled a sufficient absorption of X-rays to distinguish between fungal hyphae and intercalated glass microparticles on the generated 3D gray level images. Compared to talc or aluminum oxide microparticles, the spherical shape of the glass microparticles allows for easier qualitative assessment of the segmentation results. Consequentially, the following cultivation experiments utilizing glass microparticles and SR-µ-CT measurements in combination with 3D image analysis provide a platform for systematically investigating MPEC pellets.

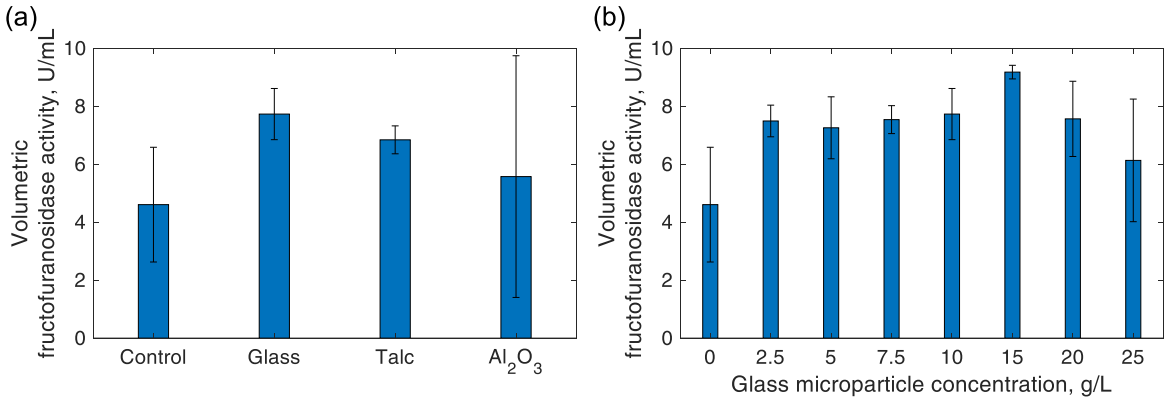

FIGURE 2 (a) Volumetric fructofuranosidase activity of a control culture (without microparticles) and microparticle-enhanced cultivation using different types of microparticles at a concentration of 10 g/L. (b) Volumetric fructofuranosidase activity for a control culture (0 g/L) and at different glass microparticle concentrations, using small glass microparticles ($x_{50,3}$ = 7.9 µm). The error bars indicate the standard deviation between supernatants of two individual cultivation flasks.

To introduce the 3D image analysis based on SR-µ-CT, three exemplary MPEC experiments were performed to investigate the fundamental effect of glass microparticle supplementation on *A. niger* cultivations. The focus was on the structural investigation over cultivation time and the impact of microparticle system characteristics, including varying concentrations and sizes.

3.1 | Influence of glass microparticle concentration on morphology

3.1.1 | Productivity and macromorphology

Pellet morphology and product synthesis in filamentous MPEC can be adjusted by the choice of the microparticle concentration (Driouch et al., 2010b; Etschmann et al., 2015; Laible et al., 2021). Thus, the global and local effects of varying concentrations of small glass microparticles (0–25 g/L) on productivity and pellet morphology were analyzed. As illustrated in Figure 2b, the addition of glass microparticles at different concentrations to cultivations of *A. niger* SKAn1015 tends to progressively enhance product activity after 72 h, with 25 g/L being an exception. However, the effect of varying glass microparticle concentrations on product activity is not strong, taking the overlapping standard deviations into account. Nevertheless, a clear increase in fructofuranosidase activity is observed at a microparticle concentration of 15 g/L (+97.8%). As previously discussed in the literature (Antecka, Bizukojc, & Ledakowicz, 2016; Driouch, Sommer, & Wittmann, 2010; Du et al., 2020; Yatmaz et al., 2020), such increases in activity and associated optimal microparticle concentrations are attributed to the impact of microparticles on the culture's morphology, e.g., affecting pellet size and pellet hyphal fraction. These observations can be confirmed in the current experiment by the 3D imaging and analysis data.

The nonsupplemented control culture has a mean VESD of 1973 µm, which decreases almost linearly with increasing concentration of glass microparticles (Figure 3a). In the approach yielding the highest product activity at 15 g/L, a mean VESD of 1262 µm was measured, while the highest microparticle concentration of 25 g/L reduced the pellet size to 520 µm. When (Driouch, Sommer, & Wittmann, 2010) added talc microparticles (x_{50} = 6 µm) to *A. niger* SKAn1015 cultivations, just 1 g/L was sufficient to grow pellets of 500 µm diameter and exclusively mycelial growth was induced at 5 g/L. However, when slightly larger talc microparticles (x_{50} = 15 µm) were used, small pellets were formed at 10 g/L. Supplementing aluminum oxide microparticles with similar size led to the formation of 500-µm pellets even at higher microparticle concentrations (15 g/L) (Driouch, Sommer, & Wittmann, 2010). A decrease in pellet size due to MPEC was also observed for *A. terreus* (Kowalska et al., 2018). In general, the reduction in pellet size, up to a certain strain-specific point, has been shown to increase the proportion of active biomass within the pellets. One reason for the increased activity is the enhanced mass transfer of essential substrates within pellets, such as oxygen, which depends on the size and density of pellets.

In addition to the VESD, the aspect ratio of the pellets significantly decreases with an increasing concentration of glass microparticles, from 0.87 to 0.44 at the highest concentration (Figure A1), which confirms the reported increase in elongation in MPEC pellets by Kowalska et al. (2018). Since the spore agglomeration is disturbed by the presence of microparticles, the morphology of the spore packages themselves becomes more heterogeneous and less spherical. Consequently, the pellets' shape also deviates further from the ideal spherical form. Furthermore, the solid and hyphal fraction in pellets with microparticles decrease in correlation with the pellet diameter with increasing glass microparticle concentration (Figure 3a). Here, the solid fraction at a microparticle concentration of 25 g/L is an exception, as the glass microparticles might constitute a majority in the initial spore-glass aggregates, which might suppress or impair further hyphal growth. Interestingly, when considering the outlier at 15 g/L (the maximum producer), it becomes evident that the sole consideration of the pellet diameter is not sufficient to evaluate the optimal morphology for peak

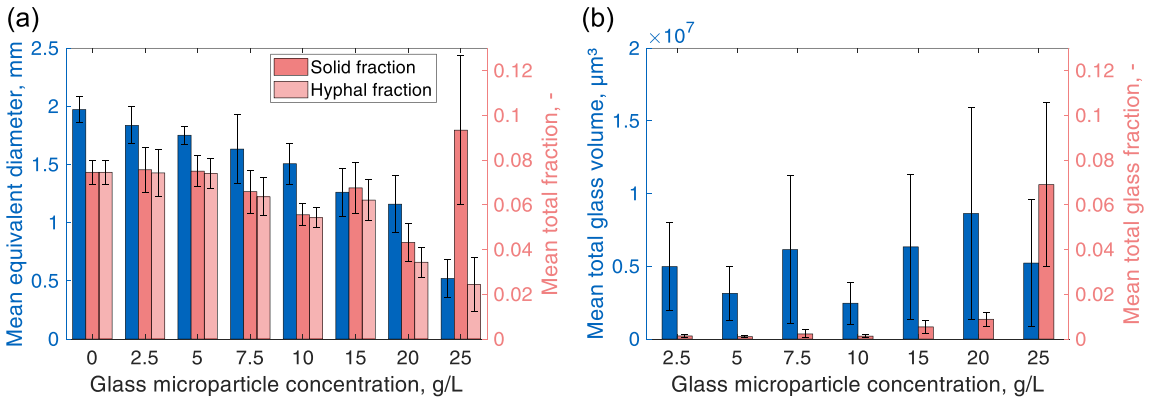

FIGURE 3 (a) Mean equivalent diameter (left ordinate), solid and hyphal fraction (right ordinate) for the control cultivation (0 g/L) and each glass microparticle concentration, and (b) mean total glass volume (left ordinate) and glass fraction (right ordinate) of pellets with varying glass microparticle concentrations using small microparticles ($x_{50,3}$ = 7.9 µm). The mean values and corresponding standard deviations were calculated based on the following sample numbers for each cultivation: 4 (0 g/L), 5 (2.5 g/L), 7 (5 g/L), 6 (7.5 g/L), 9 (10 g/L), 13 (15 g/L), 13 (20 g/L), and 105 (25 g/L).

productivity. Instead, it is worthwhile to consider the solid fraction of the supplement, which might create a beneficial ratio of hyphae and the incorporated microparticles for enhanced productivity. This holistic analysis can only be provided by µ-CT analysis, as done in this work.

Figure 3b illustrates the mean total volume of glass incorporated into pellets at varying concentrations of glass microparticles. There is no clear trend among increasing glass microparticle concentrations, as the glass volume fluctuates at a similar level with a high standard deviation. However, at 25 g/L of added glass microparticles, the mean total volume of incorporated glass per pellet is similar to the total incorporated glass volume at 2.5, 7.5, or 15 g/L (Figure 3b). Additionally, microscopic images of the culture broth (data not shown) indicate that up from a microparticle concentration of 7.5 g/L there remains an increasing amount of unincorporated microparticles in the supernatant. This leads to the hypothesis that there might be a maximum amount of glass microparticles that can be incorporated in the spore-glass agglomerates within pellets. Thus, the concentration of spore-glass agglomerates/pellets in the cultivation broth increased with increasing microparticle concentration. Since the spore concentration per MPEC was the same, the spore-glass agglomerates at high concentrations have fewer spores than at lower microparticle concentrations. This might be a reason for the growth of smaller pellets with a lower total hyphal fraction (Figure 3a). Considering uniformly decreasing pellet sizes with increasing microparticle concentrations, the glass fraction of pellets increases almost exponentially with increasing microparticle concentrations. At the concentration of 25 g/L, the glass fraction even surpasses the biomass/hyphal fraction within the pellets (Figure 3b).

Although the supplementation of glass microparticles had a less pronounced effect on product formation than expected, a strong impact on the pellet macromorphology can be concluded.

3.1.2 | Glass incorporation and micromorphology

Adding microparticles to filamentous microorganisms also leads to changes in the local hyphal fractions within pellets by incorporation of these microparticles into the hyphal network (Dinius, Schrinner, et al., 2023; Driouch, Sommer, & Wittmann, 2010; Kuhl et al., 2020).

Figure 4a shows the mean local hyphal fractions from the sampled pellets of the control cultivation and MPEC with different microparticle concentrations along the radius from the pellet center

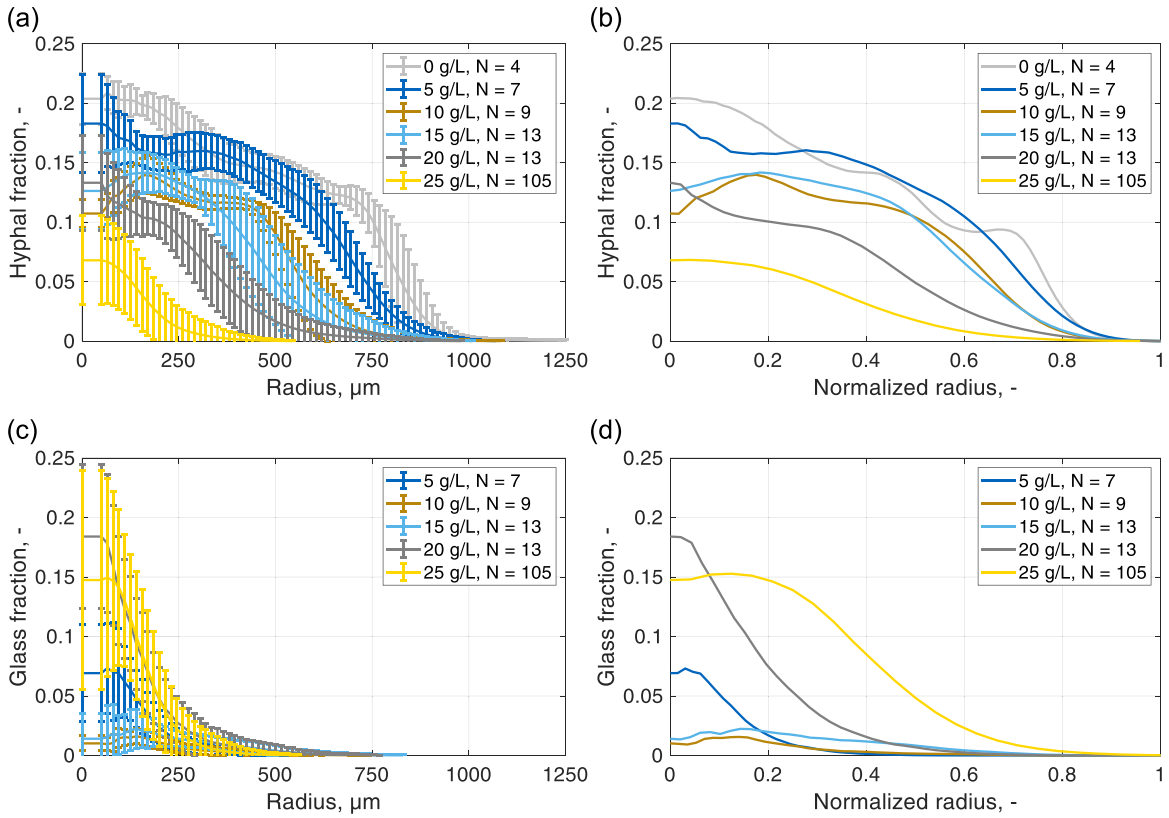

FIGURE 4 (a) Mean hyphal fractions over the pellet radius and (b) mean hyphal fractions over the normalized pellet radius. (c) Corresponding mean glass fractions over the pellet radius and (d) mean glass fractions over the normalized pellet radius at varying glass microparticle concentrations. The data points are mean values calculated with the pellet sample number (*N*) per cultivation. The error bars indicate the standard deviation between the pellets of the same sample. To obtain the normalized radius of each pellet, the distances to the pellet center were divided by the maximum distance, which corresponded to the maximum radius of the respective pellet. The measured values were then linearly interpolated to obtain equal spacing for the pellets compared with each other.

(center of mass of the pellet). Reduced hyphal fractions along the pellet radius were determined at increasing glass microparticle supplementation. Müller et al. (2023) described the center of the pellets, in which the germinated spore agglomerate is present, as the densest region of the pellets with a hyphal fraction of 20.5%–22%, which is also the case here in the control culture. All MPEC cultivations showed lower mean local hyphal fractions in the pellet core region than the control cultivation without glass microparticles.

In Figure 4b, the mean local hyphal fractions of pellets along the normalized radius (0–1) from the pellet center (center of mass of the pellet) are plotted. Clearly, higher additions of glass microparticles to *A. niger* cultivations correspond to a tendency in decreasing the overall hyphal density within pellets, particularly in the outer pellet region. These findings support hypotheses that were previously postulated based on statistically uncertain data or collected through destructive and nonrepresentative methods.

When the mean glass fractions are plotted over the pellet radius (Figure 4c), excluding the two highest glass microparticle concentrations, the highest glass fraction is located around 100 and 200 µm of the pellet radius, corresponding to the area encircling spore agglomerates. Additionally, it becomes apparent that glass microparticle presence is confined to a 300 µm radius around the pellet center, indicating that incorporation occurs within a specific timeframe during cultivation. It can be hypothesized that this might align with the size of spore-microparticle agglomerates, at which these agglomerates could become unstable regarding shear forces. These results are the first to offer 3D qualitative and quantitative insights into microparticle distributions within pellets. Compared to the conventional method of pellet slicing followed by microscopy, this approach enables higher throughput and less manual involvement, thus supporting statistical validation.

Furthermore, insights derived from the 3D data analysis enable the determination of the glass fraction across the normalized pellet radius (Figure 4d). A large accumulation of microparticles at the pellet center becomes evident at the lowest (5 g/L) and highest concentrations (20 and 25 g/L). These accumulations subsequently decrease along the pellet radius. At higher microparticle concentrations (15–25 g/L), the glass microparticles significantly occupy more than half of the pellet radius (60%–80%). Lower microparticle concentrations (<10 g/L) are mostly limited to 40% of the maximum pellet radius. Similar patterns of incorporation variations were observed in 2D microscopic images described in (Driouch et al., 2012).

Depending on the microparticle concentration, MPEC exhibits a reduction in the density of the hyphal network, reaching an optimal point. If the added microparticle concentration is too high, the hyphal fraction in a pellet could be reduced too much, for example, below 10% at 25 g/L (Figure 4a,b), whereas the glass fraction in the pellet increases too much along the radius (Figure 4c,d), which may have a detrimental effect on productivity. In addition, an increase in the microparticle concentration appears to lead to a higher concentration of spore-glass agglomerates, assumably caused by the aforementioned increased instability. This shift is observed alongside a lower fraction of spores per spore agglomerate at a constant spore concentration.

To the best of our knowledge, these findings mark the first precise quantification of incorporated microparticles within MPEC for individual pellets, as otherwise, the separation of biomass and microparticles is challenging and nearly impossible without destroying the biomass.

3.2 | Global morphology development of MPEC pellets

3.2.1 | Macromorphology

To track the development of pellets in a nonsupplemented control culture compared to MPEC with small microparticles (10 g/L), samples were taken after 24, 48, and 72 h of cultivation (Figure 5). The sample from the MPEC approach at 24 h did not yield pellets

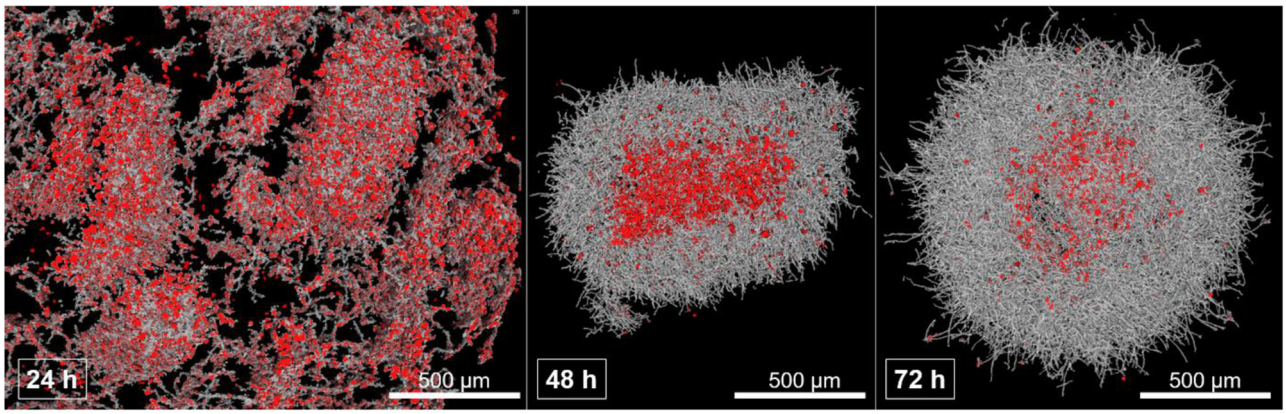

FIGURE 5 Pellet development after 24, 48, and 72 h of cultivation. Pellets from microparticle-enhanced cultivation using small glass microparticles ($x_{50,3}$ = 7.9 µm) at a microparticle concentration of 10 g/L. The segmented microparticles are shown in red. The images were generated with synchrotron radiation-based microcomputed tomography of freeze-dried pellet samples. Image processing, including segmentation of pellets, was performed with MATLAB.

yet; instead, it showed agglomerates of glass microparticles (red color) and dispersed mycelium (gray color) (Figure 5, left). Therefore, no quantitative morphological data can be presented for this sample point. It can be assumed that the presence of glass microparticles disturbed the spore agglomeration, leading to a noticeable delay in pellet formation and glucose consumption (data not shown). Accordingly, (Kowalska et al., 2018) observed the agglomerates in the early agglomeration phase of MPEC in *Aspergillus terreus* to be significantly smaller than in the control culture. This hypothesis can also be supported by the samples collected at 48 h, where the MPEC pellets (1096 µm) exhibit significantly smaller VESD than the control pellets (1287 µm) (Figure 6a). By the 72 h of cultivation mark, the VESD of the control pellets had reached 1368 µm, while the mean size of MPEC pellets was 721 µm (Figure 6a). However, despite analyzing a comparably large sample size of 19, this value is unlikely to represent the cultivation in general. This is due to its quite pellet small size in comparison to other experimental approaches conducted under the same conditions (see Figure 3a). A potential reason could include discrepancies in handling the shaking flask of this particular sample. Likewise, other sources of error as breakage of pellets associated with the freeze-drying procedure, mishandling in the course of sample preparation, or a nonrepresentative filling of the sample holder for SR-µ-CT measurements cannot be fully excluded. Nevertheless, when considering the results from other experiments, it becomes evident that pellet growth is notably delayed, and the pellet sizes are consistently reduced over the course of the entire cultivation time. The analysis of the total glass volume and glass fraction (Figure 6b) is also consistent with the hypothesis of a nonrepresentative sample at 72 h. Unexpectedly, the incorporated glass volume decreases significantly from the sample at 48–72 h, while the glass fraction remains nearly constant. Since no significant destruction of the pellet is expected at the beginning of the stationary growth phase (72 h of cultivation), such a severe decrease in total glass incorporation is also implausible.

3.2.2 | Glass incorporation and micromorphology

Examining the local hyphal fractions in the nonsupplemented control culture (Figure 7a,b), the plot illustrates a comparably low hyphal density at 24 h. In general, the course of this specific sample exhibits similarities to the observations discussed in (Müller et al., 2023). Notably, the mean hyphal fraction at 24 h at the center of the pellets (12%) holds around half the value compared to the pellets in Müller et al. (2023) (22%), and the hyphal fraction constantly converges to zero at a larger radius. As growth progresses, the hyphal fractions for 48 and 72 h demonstrate a similar, upwards-shifted trend, exhibiting a fluctuating decrease over time. The hyphal fractions for both time points are reduced compared to the data presented in (Müller et al., 2023). However, in this study, for each experiment considered individually, the effect of densification over the entire pellet radius throughout the cultivation time appears to be more pronounced. After 48 h, the mean hyphal fractions in outer regions of the MPEC pellets are smaller than the hyphal fractions of the pellets from the nonsupplemented control cultivation. After 72 h, the local hyphal fractions of the MPEC pellets are clearly reduced throughout the pellet radius compared to the unsupplemented control cultivation. Such a MPEC-induced decrease in hyphal density could potentially contribute to an improved nutrition supply and enhanced product formation, suggesting a beneficial effect. Consequently, higher productivity of MPECs results from an interplay between mass transfer, hyphal fraction, glass fraction, and solid fraction within pellets. Similar to the hyphal fraction the glass fractions also decrease after the 72 h of cultivation mark compared to the MPEC pellets after 48 h, potentially caused by breakage of the

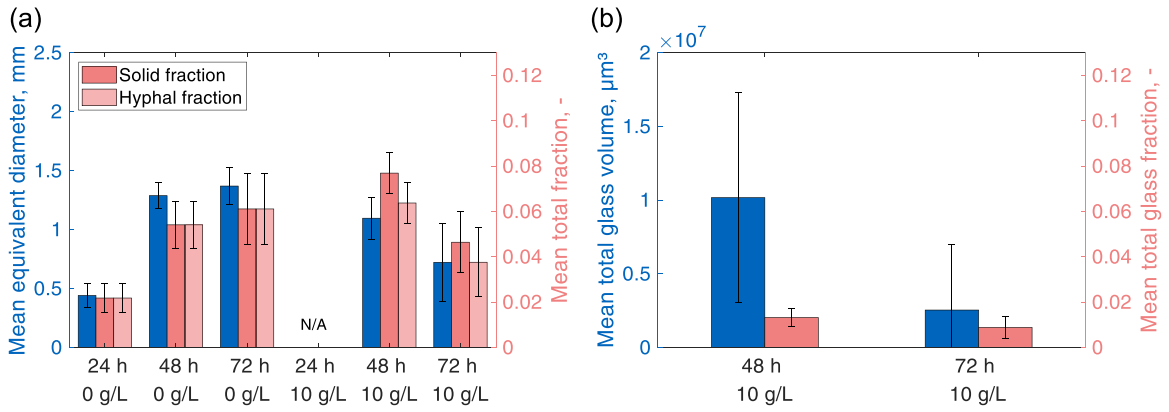

FIGURE 6 (a) Time-resolved mean equivalent diameter, solid, and hyphal fraction for the control cultivation (24–72 h) and microparticle-enhanced cultivation with a glass microparticle ($x_{50,3}$ = 7.9 µm) concentration of 10 g/L on a daily sampling basis, and (b) mean total glass volume and glass fraction intercalated within the pellets at 48 and 72 h of cultivation. The mean values and corresponding standard deviations were calculated based on the following sample numbers for each cultivation: 72 (24 h, 0 g/L), 14 (48 h, 0 g/L), 11 (72 h, 0 g/L), 22 (48 h, 10 g/L), and 19 (72 h, 10 g/L).

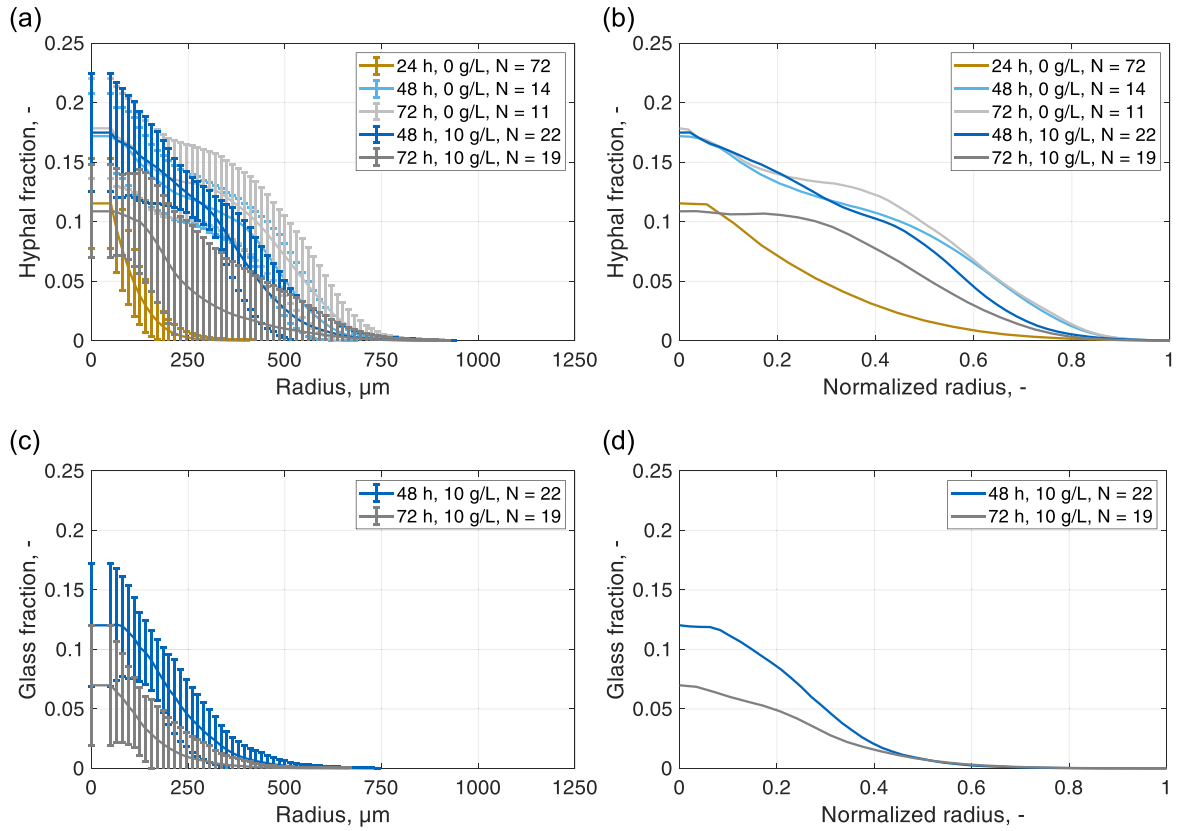

FIGURE 7 (a) Mean hyphal fractions over the pellet radius and (b) mean hyphal fractions over the normalized pellet radius. (c) Corresponding mean glass fractions over the pellet radius and (d) mean glass fractions over the normalized pellet radius on a daily sampling basis. The data points are mean values calculated with the pellet sample number (*N*) for each cultivation. The error bars indicate the standard deviation between the pellets of the same sample. To obtain the normalized radius of each pellet, the distances to the pellet center were divided by the maximum distance, which corresponded to the maximum radius of the respective pellet. The measured values were then linearly interpolated to obtain equal spacing for the pellets compared with each other.

spore-glass agglomerates/pellets. At 48 h, the glass microparticles are found up to a radius of 500 µm, while at 72 h, they are present to an approximate radius of 350 µm (Figure 7c). The incorporation of glass microparticles after 48 and 72 h corresponds to a normalized radius of up to 0.6 (Figure 7d).

In conclusion, it can be noted that "young" pellets without microparticles exhibit a uniformly declining course in hyphal fraction. As the pellets age and grow during cultivation, as previously discussed by Müller et al. (2023), the level of heterogeneity increases, as indicated by the increased standard deviations in the mean hyphal fraction after 48 and 72 h (Figure 7a). Additionally, the influence of the supplemented glass microparticles is another source of heterogeneity, leading to more fluctuations of hyphal fractions over the radius.

3.3 | Influence of glass microparticle size on pellet morphology

In another experiment, differences in the incorporation behavior and the effects of small glass microparticles ($x_{50,3}$ = 7.9 µm) compared to large microparticles ($x_{50,3}$ = 30.5 µm) on the inner pellet structure were elucidated.

3.3.1 | Macromorphology

The pellet size of the nonsupplemented control culture in this experiment is higher compared to all other nonsupplemented control cultures (Figure 8a). Further, it can be observed that the impact of glass microparticle incorporation on pellet size diminishes when larger glass particles are added. For both microparticle sizes, an increase in microparticle concentration further reduces the resulting pellet sizes, although the difference is more pronounced for the large microparticles. In a previous study, (Driouch, Sommer, & Wittmann, 2010) already concluded that smaller microparticles have a stronger effect on cultivations of *A. niger* SKAn1015. There, smaller talc microparticles (6 µm) evoked the formation of dispersed mycelium, while the supplementation of larger talc microparticles (15 µm) at the same concentration (10 g/L) resulted in the formation of small pellets. In their study, the authors only proposed that the general mechanism of the

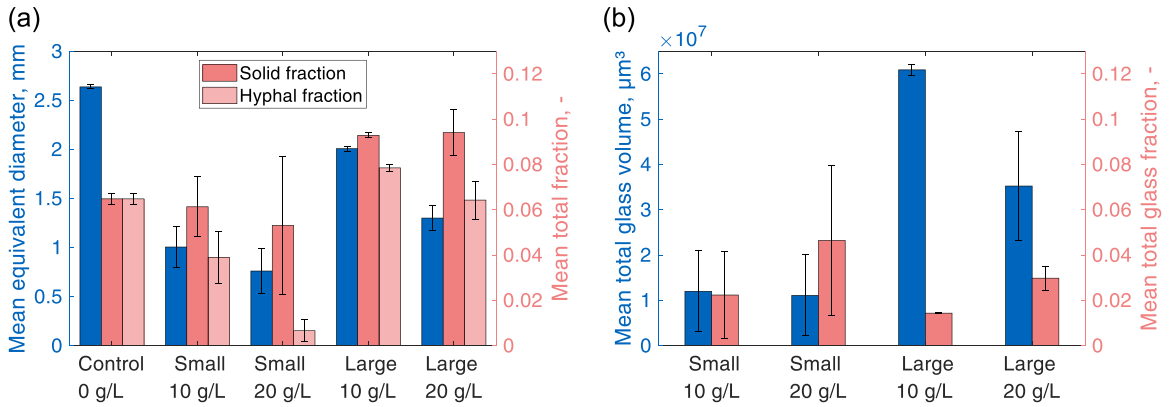

FIGURE 8 (a) Mean equivalent diameter, solid, and hyphal fraction for the control cultivation and microparticle-enhanced cultivation with small ($x_{50,3}$ = 7.9 µm) and large ($x_{50,3}$ = 30.5 µm) microparticles at a concentration of 10 and 20 g/L and (b) mean total glass volume and glass fraction intercalated within the pellets at varying microparticles sizes and concentrations. The mean values and corresponding standard deviations were calculated based on the following sample numbers for each cultivation: 2 (0 g/L), 23 (small, 10 g/L), 39 (small, 20 g/L), 2 (large, 10 g/L), and 9 (large, 20 g/L).

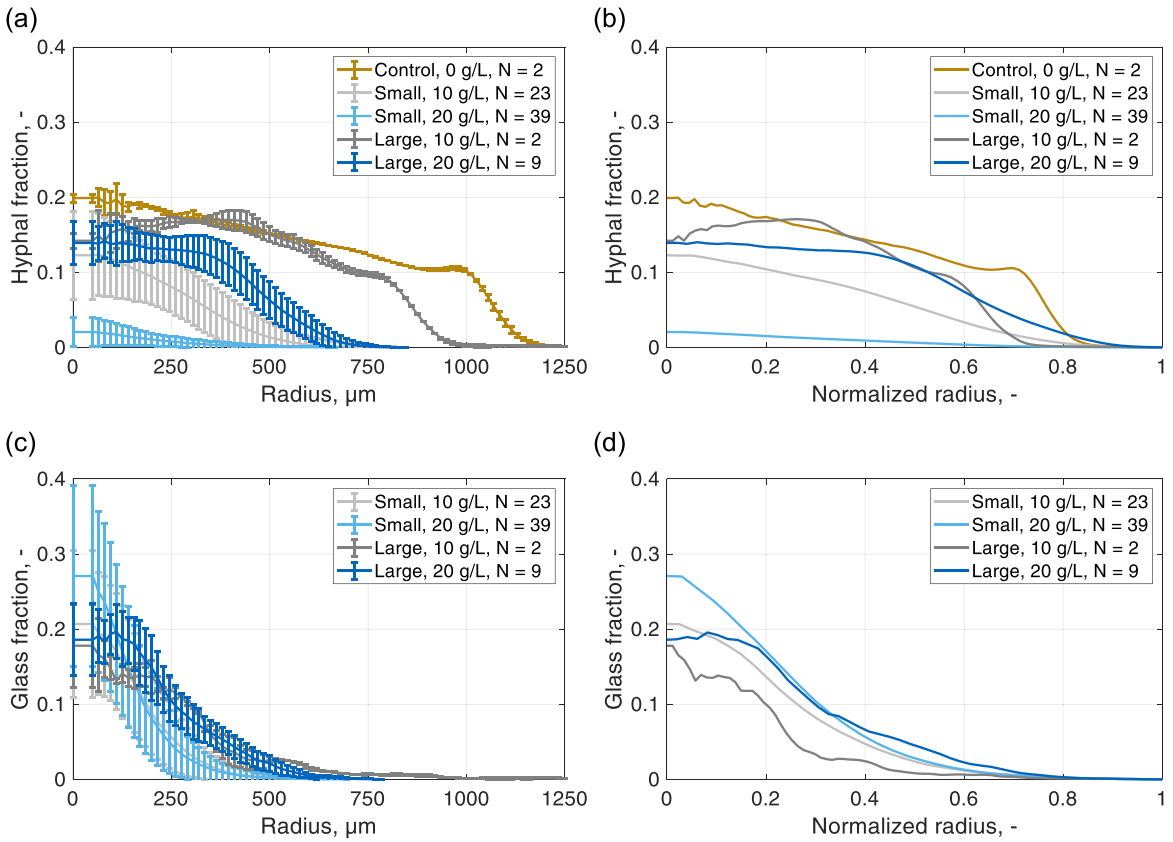

FIGURE 9 (a) Mean hyphal fractions over the pellet radius and (b) mean hyphal fractions over the normalized pellet radius. (c) Corresponding mean glass fractions over the pellet radius and (d) mean glass fractions over the normalized pellet radius with small and big microparticle at a concentration of 10 and 20 g/L. The data points are mean values calculated with the pellet sample number (*N*) per cultivation. The error bars indicate the standard deviation between the pellets of the same sample. To obtain the normalized radius of each pellet, the distances to the pellet center were divided by the maximum distance, which corresponded to the maximum radius of the respective pellet. The measured values were then linearly interpolated to obtain equal spacing for the pellets compared with each other.

microparticle effect is the disturbance of the initial spore aggregation. However, the specific characteristics of small or large microparticles, respectively, were not discussed. Furthermore, the overall solid and hyphal fraction of pellets supplemented with small and large glass microparticles is also depicted in Figure 8a. It can be concluded that, regardless of the microparticle size, the total hyphal fraction of MPEC pellets decreases with increasing particle concentration, and the effect is more pronounced for MPEC with smaller microparticles.

3.3.2 | Glass incorporation and micromorphology

By analyzing the hyphal fraction (Figure 9a,b) a consistent trend can be confirmed: the addition of microparticles reduces the overall hyphal fraction across the entire pellet radius compared to the nonsupplemented control cultivation. Moreover, higher microparticle concentrations in each case lead to a more significant decrease in the hyphal fraction. Additionally, it can be determined that the local hyphal fractions are smaller as the microparticle size decreases. This might be caused by the increasing impact of small microparticles on spore aggregation and pellet evolution.

A discernable trend can be observed in the 3D images of the pellets supplemented with large glass microparticles: specific microparticles tend to be preferentially incorporated at certain pellet radii (compare Figure 1a). While the smaller fraction of the large ($x_{50,3}$ = 30.5 µm) glass microparticles is predominantly located in the pellet center rather than the outer pellet region, the trend is reversed for larger microparticles. Figure 1b shows an MPEC pellet with small glass microparticles, which are almost exclusively embedded in the pellet center. Compared to the large microparticles, the total glass volume of the small microparticles is significantly lower at both added concentrations (10 and 20 g/L), as shown in Figure 8b. However, the larger microparticles are distributed more extensively throughout the pellets, as demonstrated by the local glass fractions (Figure 9c,d). Therefore, even though many microparticles are incorporated into the pellets, the large microparticles do not seem to play a role in disturbing the initial spore aggregation. Thereby, fewer spores might be substituted by glass microparticles within spore-glass agglomerates. Thus, due to spore-glass agglomerates with fewer (large) glass microparticles during pellet development, the resulting pellets with large microparticles obtain a higher VESD and are overall denser (Figures 8a,b and 9a,b). This confirms the hypothesis of (Antecka et al., 2016a), who proposed that microparticles comparable to the size of spores were the most efficient at altering fungal morphology. From these results, it can be hypothesized that there may be a specific particle size threshold between 20 and 50 µm. Larger microparticles no longer appear to impair spore agglomeration during the initial cultivation phase. Furthermore, the similar total glass volume of the incorporated small glass microparticles at both added concentrations (see Figure 8b) enforces the hypothesis in Section 3.1.-2 that only a certain maximum of glass microparticles can be stored within spore-glass agglomerates in the pellets.

The local glass fractions are high compared to the other experiments (compare Figure 9c and Figure 9d). While the small microparticles exhibit an exponential decrease in glass content, both concentrations reach a pellet radius of approximately 500 µm (Figure 9c). Contrary, the decrease is more erratic for the large microparticles, with fluctuations at a small scale. For both glass microparticle sizes and concentrations, the glass fraction approaches zero at a normalized radius of approximately 0.7 (Figure 9d). The overall mean pellet size is larger for larger glass microparticles. In addition, small microparticles are incorporated almost exclusively in central pellet areas, whereas large microparticles are also present at higher pellet radii. Thus, a clear dependence of the incorporation behavior on the microparticle size can be determined.

4 | CONCLUSION

This study introduced glass microparticles as an effective system for MPEC in *A. niger*, enhancing the product activity. Screening experiments of *A. niger* involved SR-µ-CT measurements performed at the DESY imaging beamline P05. A developed 3D image analysis pipeline enabled the detection of incorporated glass microparticles within the pellets. For the first time, this method allowed the localization and quantification of microparticles, providing data about pellet micro- and macromorphology, such as local hyphal and glass fractions, in a nondestructive manner based on an evaluation of 375 pellets. So far, the fundamental mechanisms of MPEC and other morphology engineering approaches are not yet fully understood. Therefore, this kind of 3D analysis paves the way to comprehensively understand the pellet micro- and macromorphological impact, for example, of various microparticles. Here, even different types of microparticles, such as talc or aluminum oxide can be detected. The generated data can, for instance, be integrated into modeling approaches to predict filamentous microorganisms' growth and substrate supply under varying cultivation conditions.

The analysis of MPEC with varying glass microparticle concentrations revealed a strong correlation between increasing microparticle concentration and decreasing pellet sizes, as well as the specific incorporated glass volume. Monitoring the 3D pellet growth confirmed previous hypotheses regarding reduced hyphal fractions due to microparticle addition. Furthermore, compared to nonsupplemented control cultivations, MPEC samples exhibit a significant delay in pellet formation, probably attributed to the disruption of the spore agglomeration in the early pellet formation by the microparticles. Moreover, as pellets aged, they were subject to densification and exhibited increasingly heterogenous micromorphologies in conjunction with microparticle supplementation. It was further confirmed that the impact of MPEC was more pronounced for smaller microparticles of the same type,

presumably due to their more substantial impact on the initial spore agglomeration. These results, derived from the data of our developed method, can contribute to the further development of MPEC in future research and support industrial application.

AUTHOR CONTRIBUTIONS

Henri Müller and Anna Dinius did the conception and design of the study. Anna Dinius and Henri Müller wrote the manuscript, which was edited and approved by all authors. Heiko Briesen and Rainer Krull supervised the study. Anna Dinius cultivated filamentous fungi and prepared pellets for microcomputed tomography (SR-µ-CT) measurements. Jörg U. Hammel, Henri Müller, Anna Dinius, Stefan Schmideder, and Charlotte Deffur performed SR-µ-CT measurements of pellets. Jörg U. Hammel and Henri Müller reconstructed the image data. Henri Müller and Diana Kellhammer created the code for image analysis. Henri Müller and Diana Kellhammer performed the image and data processing. Henri Müller created the figures. Anna Dinius, Henri Müller, Rainer Krull, Heiko Briesen, and Diana Kellhammer interpreted the data.

ACKNOWLEDGMENTS

The authors acknowledge DESY (Hamburg, Germany), a member of the Helmholtz Association HGF, for providing experimental facilities. The authors acknowledge provision of beamtime, related to the proposals I—20211150 and I—20200214 at the Imaging Beamline P05 at PETRA III at DESY, a member of the Helmholtz Association (HGF). This research was supported in part by the Maxwell computational resources operated at Deutsches Elektronen-Synchrotron DESY, Hamburg, Germany. Furthermore, the authors thank Kilian Lupp for preliminary image analysis and data processing studies. Moreover, the authors thank Lars Barthel and Karin Engelbert (Department of Applied and Molecular Microbiology, Institute of Biotechnology, Technische Universität Berlin, Germany) for assisting the SR-µ-CT measurements. The authors thank the Deutsche Forschungsgemeinschaft for financial support for this study within the SPP 1934 DiSPBiotech—315384307, 315305620, and 31547657 and SPP2170 InterZell—427889137. Open Access funding enabled and organized by Projekt DEAL.

CONFLICT OF INTEREST STATEMENT

The authors declare no conflicts of interest.

DATA AVAILABILITY STATEMENT

The data that support the findings of this study are available from the corresponding author upon reasonable request.

ORCID

Anna Dinius http://orcid.org/0000-0002-3562-7925
Henri Müller http://orcid.org/0000-0002-4831-0003
Diana Kellhammer http://orcid.org/0009-0009-4883-5027
Charlotte Deffur http://orcid.org/0000-0002-3902-0602
Stefan Schmideder http://orcid.org/0000-0003-4328-9724
Jörg U. Hammel http://orcid.org/0000-0002-6744-6811
Rainer Krull http://orcid.org/0000-0003-2821-8610
Heiko Briesen http://orcid.org/0000-0001-7725-5907

REFERENCES

Van Aarle, W., Palenstijn, W. J., De Beenhouwer, J., Altantzis, T., Bals, S., Batenburg, K. J., & Sijbers, J. (2015). The ASTRA toolbox: A platform for advanced algorithm development in electron tomography. *Ultramicroscopy*, *157*, 35–47. https://doi.org/10.1016/j.ultramic.2015.05.002

Van Aarle, W., Palenstijn, W. J., Cant, J., Janssens, E., Bleichrodt, F., Dabravolski, A., De Beenhouwer, J., Joost Batenburg, K., & Sijbers, J. (2016). Fast and flexible X-ray tomography using the ASTRA toolbox. *Optics Express*, *24*(22), 25129–25147. https://doi.org/10.1364/OE.24.025129

Antecka, A., Bizukojc, M., & Ledakowicz, S. (2016). Modern morphological engineering techniques for improving productivity of filamentous fungi in submerged cultures. *World Journal of Microbiology and Biotechnology*, *32*, 193. https://doi.org/10.1007/s11274-016-2148-7

Antecka, A., Blatkiewicz, M., Bizukojć, M., & Ledakowicz, S. (2016). Morphology engineering of basidiomycetes for improved laccase biosynthesis. *Biotechnology Letters*, *38*(4), 667–672. https://doi.org/10.1007/s10529-015-2019-6

Bizukojc, M., & Ledakowicz, S. (2010). The morphological and physiological evolution of *Aspergillus terreus* mycelium in the submerged culture and its relation to the formation of secondary metabolites. *World Journal of Microbiology and Biotechnology*, *26*, 41–54. https://doi.org/10.1007/s11274-009-0140-1

Böl, M., Schrinner, K., Tesche, S., & Krull, R. (2021). Challenges of influencing cellular morphology by morphology engineering techniques and mechanical induced stress on filamentous pellet systems—A critical review. *Engineering in Life Sciences*, *21*(3–4), 51–67. https://doi.org/10.1002/elsc.202000060

Cairns, T. C., Nai, C., & Meyer, V. (2018). How a fungus shapes biotechnology: 100 years of *Aspergillus niger* research. *Fungal Biology and Biotechnology*, *5*, 13. https://doi.org/10.1186/s40694-018-0054-5

Cairns, T. C., Zheng, X., Zheng, P., Sun, J., & Meyer, V. (2019). Moulding the mould: Understanding and reprogramming filamentous fungal growth and morphogenesis for next generation cell factories. *Biotechnology for Biofuels*, *12*, 77. https://doi.org/10.1186/s13068-019-1400-4

Colin, V. L., Baigorí, M. D., & Pera, L. M. (2013). Tailoring fungal morphology of *Aspergillus niger* MYA 135 by altering the hyphal morphology and the conidia adhesion capacity: Biotechnological applications. *AMB Express*, *3*, 27. https://doi.org/10.1186/2191-0855-3-27

Dinius, A., Kozanecka, Z. J., Hoffmann, K. P., & Krull, R. (2023). Intensification of bioprocesses with filamentous microorganisms. *Physical Sciences Reviews*, *9*(2), 777–823. https://doi.org/10.1515/psr-2022-0112

Dinius, A., Schrinner, K., Schrader, M., Kozanecka, Z. J., Brauns, H., Klose, L., Weiß, H., Kwade, A., & Krull, R. (2023). Morphology engineering for novel antibiotics: Effect of glass microparticles and soy lecithin on rebeccamycin production and cellular morphology of filamentous actinomycete *Lentzea aerocolonigenes*. *Frontiers in Bioengineering and Biotechnology*, *11*, 1171055. https://doi.org/10.3389/fbioe.2023.1171055

Driouch, H., Hänsch, R., Wucherpfennig, T., Krull, R., & Wittmann, C. (2012). Improved enzyme production by bio-pellets of *Aspergillus niger*: Targeted morphology engineering using titanate microparticles. *Biotechnology and Bioengineering*, *109*(2), 462–471. https://doi.org/10.1002/bit.23313

Driouch, H., Roth, A., Dersch, P., & Wittmann, C. (2010). Optimized bioprocess for production of fructofuranosidase by recombinant *Aspergillus niger*. *Applied Microbiology and Biotechnology*, *87*, 2011–2024. https://doi.org/10.1007/s00253-010-2661-9

Driouch, H., Sommer, B., & Wittmann, C. (2010). Morphology engineering of *Aspergillus niger* for improved enzyme production. *Biotechnology and Bioengineering*, *105*(6), 1058–1068. https://doi.org/10.1002/bit.22614

Du, L., Gao, B., Liang, J., Wang, Y., Xiao, Y., & Zhu, D. (2020). Microparticle-enhanced *Chaetomium globosum* DX-THS3 β-d-glucuronidase production by controlled fungal morphology in submerged fermentation. *3 Biotech*, *10*(3):100. https://doi.org/10.1007/s13205-020-2068-y

Etschmann, M. M. W., Huth, I., Walisko, R., Schuster, J., Krull, R., Holtmann, D., Wittmann, C., & Schrader, J. (2014). Improving 2-phenylethanol and 6-pentyl-α-pyrone production with fungi by microparticle-enhanced cultivation (MPEC): Microparticle-enhanced cultivation for flavour production in fungi. *Yeast*, *32*. https://doi.org/10.1002/yea.3022

Füting, P., Barthel, L., Cairns, T. C., Briesen, H., & Schmideder, S. (2021). Filamentous fungal applications in biotechnology: A combined bibliometric and patentometric assessment. *Fungal Biology and Biotechnology*, *8*(1):23. https://doi.org/10.1186/s40694-021-00131-6

Gonciarz, J., & Bizukojc, M. (2014). Adding talc microparticles to *Aspergillus terreus* ATCC 20542 preculture decreases fungal pellet size and improves lovastatin production. *Engineering in Life Sciences*, *14*(2), 190–200. https://doi.org/10.1002/elsc.201300055

Greving, I., Wilde, F., Ogurreck, M., Herzen, J., Hammel, J. U., Hipp, A., & Beckmann, F. (2014). P05 imaging beamline at PETRA III: First results. In S. R. Stock (Ed.), *SPIE proceedings*, *developments in X-ray tomography IX*. 92120O. https://doi.org/10.1117/12.2061768

Gürler, H. N., Erkan, S. B., Ozcan, A., Yılmazer, C., Karahalil, E., Germec, M., Yatmaz, E., Ogel, Z. B., & Turhan, I. (2021). Scale-up processing with different microparticle agent for β-mannanase production in a large-scale stirred tank bioreactor. *Journal of Food Processing and Preservation*, *45*(8), e14915. https://doi.org/10.1111/jfpp.14915

Haibel, A., Ogurreck, M., Beckmann, F., Dose, T., Wilde, F., Herzen, J., & Mohr, J. (2010). Micro- and nano-tomography at the GKSS Imaging Beamline at PETRA III. In S. R. Stock (Ed.), *SPIE proceedings*, *developments in X-ray tomography*. VII (78040B). https://doi.org/10.1117/12.860852

Kaup, B.-A., Ehrich, K., Pescheck, M., & Schrader, J. (2008). Microparticle-enhanced cultivation of filamentous microorganisms: Increased chloroperoxidase formation by *Caldariomyces fumago* as an example. *Biotechnology and Bioengineering*, *99*(3), 491–498. https://doi.org/10.1002/bit.21713

Kowalska, A., Boruta, T., & Bizukojć, M. (2018). Morphological evolution of various fungal species in the presence and absence of aluminum oxide microparticles: Comparative and quantitative insights into microparticle-enhanced cultivation (MPEC). *MicrobiologyOpen*, *7*, e00603. https://doi.org/10.1002/mbo3.603

Krull, R., Wucherpfennig, T., Esfandabadi, M. E., Walisko, R., Melzer, G., Hempel, D. C., Kampen, I., Kwade, A., & Wittmann, C. (2013). Characterization and control of fungal morphology for improved production performance in biotechnology. *Journal of Biotechnology*, *163*, 112–123. https://doi.org/10.1016/j.jbiotec.2012.06.024

Kuhl, M., Gläser, L., Rebets, Y., Rückert, C., Sarkar, N., Hartsch, T., Kalinowski, J., Luzhetskyy, A., & Wittmann, C. (2020). Microparticles globally reprogram *Streptomyces albus* toward accelerated morphogenesis, streamlined carbon core metabolism, and enhanced production of the antituberculosis polyketide pamamycin. *Biotechnology and Bioengineering*, *117*, 3858–3875. https://doi.org/10.1002/bit.27537

Laible, A. R., Dinius, A., Schrader, M., Krull, R., Kwade, A., Briesen, H., & Schmideder, S. (2021). Effects and interactions of metal oxides in microparticle-enhanced cultivation of filamentous microorganisms. *Engineering in Life Sciences*, *22*, 725–743. https://doi.org/10.1002/elsc.202100075

Lin, P.-J., Scholz, A., & Krull, R. (2010). Effect of volumetric power input by aeration and agitation on pellet morphology and product formation of *Aspergillus niger*. *Biochemical Engineering Journal*, *49*, 213–220. https://doi.org/10.1016/j.bej.2009.12.016

Meyer, F. (1994). Topographic distance and watershed lines. *Signal Processing*, *38*(1), 113–125. https://doi.org/10.1016/0165-1684(94)90060-4

Moosmann, J., Ershov, A., Weinhardt, V., Baumbach, T., Prasad, M. S., LaBonne, C., Xiao, X., Kashef, J., & Hofmann, R. (2014). Time-lapse X-ray phase-contrast microtomography for in vivo imaging and analysis of morphogenesis. *Nature Protocols*, *9*(2), 294–304. https://doi.org/10.1038/nprot.2014.033

Müller, H., Deffur, C., Schmideder, S., Barthel, L., Friedrich, T., Mirlach, L., Hammel, J. U., Meyer, V., & Briesen, H. (2023). Synchrotron radiation-based microcomputed tomography for three-dimensional growth analysis of *Aspergillus niger* pellets. *Biotechnology and Bioengineering*, *120*, 3244–3260. https://doi.org/10.1002/bit.28506

Otsu, N. (1979). A threshold selection method from gray-Level histograms. *IEEE Transactions on Systems, Man and Cybernetics*, *9*, 62–66. https://doi.org/10.1109/TSMC.1979.4310076

Palenstijn, W. J., Batenburg, K. J., & Sijbers, J. (2011). Performance improvements for iterative electron tomography reconstruction using graphics processing units (GPUs). *Journal of Structural Biology*, *176*(2), 250–253. https://doi.org/10.1016/j.jsb.2011.07.017

Papagianni, M., & Mattey, M. (2006). Morphological development of *Aspergillus niger* in submerged citric acid fermentation as a function of the spore inoculum level. Application of neural network and cluster analysis for characterization of mycelial morphology. *Microbial Cell Factories*, *5*, 3. https://doi.org/10.1186/1475-2859-5-3

Posch, A. E., Spadiut, O., & Herwig, C. (2012). A novel method for fast and statistically verified morphological characterization of filamentous fungi. *Fungal Genetics and Biology*, *49*(7), 499–510. https://doi.org/10.1016/j.fgb.2012.05.003

Schmideder, S., Barthel, L., Friedrich, T., Thalhammer, M., Kovačević, T., Niessen, L., Meyer, V., & Briesen, H. (2019). An X-ray microtomography-based method for detailed analysis of the three-dimensional morphology of fungal pellets. *Biotechnology and Bioengineering*, *116*(6), 1355–1365. https://doi.org/10.1002/bit.26956

Schmideder, S., Barthel, L., Müller, H., Meyer, V., & Briesen, H. (2019). From three-dimensional morphology to effective diffusivity in filamentous fungal pellets. *Biotechnology and Bioengineering*, *116*(12), 3360–3371. https://doi.org/10.1002/bit.27166

Schmideder, S., Müller, H., Barthel, L., Friedrich, T., Niessen, L., Meyer, V., & Briesen, H. (2021). Universal law for diffusive mass transport through mycelial networks. *Biotechnology and Bioengineering*, *118*(2), 930–943. https://doi.org/10.1002/bit.27622

Schrinner, K., Veiter, L., Schmideder, S., Doppler, P., Schrader, M., Münch, N., Althof, K., Kwade, A., Briesen, H., Herwig, C., & Krull, R. (2020). Morphological and physiological characterization of filamentous *Lentzea aerocolonigenes*: Comparison of biopellets by

microscopy and flow cytometry. *PLoS One*, *15*(6), e0234125. https://doi.org/10.1371/journal.pone.0234125

Veiter, L., Rajamanickam, V., & Herwig, C. (2018). The filamentous fungal pellet-relationship between morphology and productivity. *Applied Microbiology and Biotechnology*, *102*(7), 2997–3006. https://doi.org/10.1007/s00253-018-8818-7

Wilde, F., Ogurreck, M., Greving, I., Hammel, J. U., Beckmann, F., Hipp, A., & Schreyer, A. (2016). *Micro-CT at the imaging beamline P05 at PETRA III 030035*. In AIP Conference Proceedings (Vol. 1741):30035. https://doi.org/10.1063/1.4952858

Wösten, H. A. B. (2019). Filamentous fungi for the production of enzymes, chemicals and materials. *Current Opinion in Biotechnology*, *59*, 65–70. https://doi.org/10.1016/j.copbio.2019.02.010

Wucherpfennig, T., Hestler, T., & Krull, R. (2011). Morphology engineering - osmolality and its effect on *Aspergillus niger* morphology and productivity. *Microbial Cell Factories*, *10*, 58. https://doi.org/10.1186/1475-2859-10-58

Wucherpfennig, T., Kiep, K. A., Driouch, H., Wittmann, C., & Krull, R. (2010). Morphology and rheology in filamentous cultivations. *Advances in Applied Microbiology*, *72*, 89–136. https://doi.org/10.1016/S0065-2164(10)72004-9

Yatmaz, E., Germec, M., Karahalil, E., & Turhan, I. (2020). Enhancing β-mannanase production by controlling fungal morphology in the bioreactor with microparticle addition. *Food and Bioproducts Processing*, *121*, 123–130. https://doi.org/10.1016/j.fbp.2020.02.003

Yatmaz, E., Karahalil, E., Germec, M., Ilgin, M., & Turhan, I. (2016). Controlling filamentous fungi morphology with microparticles to enhanced β-mannanase production. *Bioprocess and Biosystems Engineering*, *39*(9), 1391–1399. https://doi.org/10.1007/s00449-016-1615-8

Zuccaro, A., Götze, S., Kneip, S., Dersch, P., & Seibel, J. (2008). Tailor-made fructooligosaccharides by a combination of substrate and genetic engineering. *ChemBioChem*, *9*, 143–149. https://doi.org/10.1002/cbic.200700486

How to cite this article: Dinius, A., Müller, H., Kellhammer, D., Deffur, C., Schmideder, S., Hammel, J. U., Krull, R., & Briesen, H. (2024). 3D imaging and analysis to unveil the impact of microparticles on the pellet morphology of filamentous fungi. *Biotechnology and Bioengineering*, *121*, 3128–3143. https://doi.org/10.1002/bit.28788

APPENDIX

Figure A1

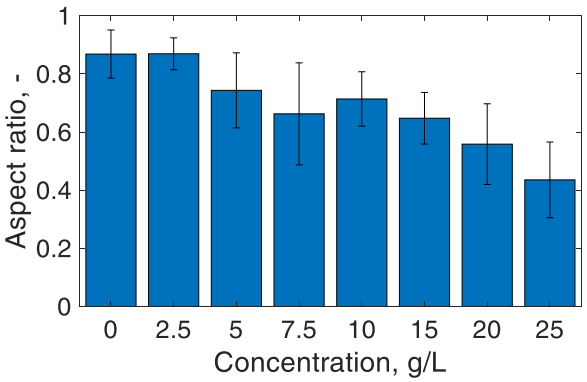

FIGURE A1 Aspect ratio of *Aspergillus niger* pellets from microparticle-enhanced cultivation with small glass microparticles ($x_{50,3}$ = 7.9 µm) at various microparticle concentrations determined after 72 h of cultivation.